Metal–Organic Frameworks

DOI: 10.1002/anie.201203929

Enhanced Stability in Rigid Peptide-Based Porous Materials**

*Carlos Martí-Gastaldo, John E. Warren, Kyriakos C. Stylianou, Natasha L. O. Flack, and Matthew J. Rosseinsky**

Metal–organic frameworks (MOFs) are a class of crystalline materials built up from the interconnection of organic linkers and metal nodes.[1] The judicious choice of these organic and inorganic synthons and the control exerted on their spatial arrangement enables fine-tuning of their intrinsic porosity and accessible surface area. This controllable structure-to-function relationship, together with their extraordinary structural and chemical versatility, have resulted in the evaluation of these porous coordination polymers in applications such as gas storage and separation,[2] heterogeneous catalysis,[3] and sensing.[4]

Within this general family, the development of open frameworks from biologically derived molecules deserves particular attention. To date, the incorporation of amino acids[5] or nucleobases[6] has been demonstrated to be a fruitful route towards the design of bio-analogous MOFs.[7]

In this context, the use of oligopeptides has recently led to adaptable porosity in $[Zn(Gly–Ala)_2]$,[8] in which the flexibility of the peptide linker adapts the pore conformation to the nature and loading of guest through its thermally accessible manifold of torsions. This scenario contrasts with that encountered in rigid frameworks, where the use of more torsionally restricted linkers limits the host ability to rearrange. We believe that a deeper understanding of the role played by more rigid dipeptide connectors is important for the development of a next generation of biomimetic porous materials since the combination of both types of components, dynamic and rigid, determines the structural flexibility in proteins and controls their folding/unfolding dynamics that determines their biological function.[9]

Here we describe $[Zn(Gly\text{-}Thr)_2]\cdot CH_3OH$ (**1**) assembled from Zn^{2+} ions and the dipeptide glycilthreonine (Gly–Thr). Besides exhibiting selective adsorption of CO_2 in preference to CH_4, this 2D layered framework displays 1D porosity and retains crystallinity upon solvent removal. This scenario contrasts with the poor structural stability generally attributed to peptide-based materials. We show how this compromise between flexibility and structural stability can be achieved by precise control of the coordination modes and supramolecular interactions enabled by the peptide, hence opening the door for the design of a next generation of robust adaptable porous materials.

Colorless crystals of **1** were isolated from the reaction of zinc nitrate and Gly-L-Thr in a methanolic solution, slightly basified with aqueous NaOH (see Supporting Information S1 for further details). This synthetic route is almost equivalent to that described for the related $[Zn(Gly–Ala)_2]$,[8] hence indicating that the synthetic versatility generally attributed to MOF chemistry can be also associated with these peptidic coordination polymers. It is worthwhile mentioning that the formation of an isomorphous hydrated phase, $\{[Zn(Gly\text{-}Thr)_2]\cdot(H_2O)_2\}_n$ (MAFGUW; Cambridge Crystallographic Data Centre number CCDC-229209), by reaction of Gly–Thr with zinc hydroxide in an aqueous medium has been previously described.[10]

Compound **1** crystallizes in the monoclinic chiral space group *I*2. Each Zn^{2+} metal center is six-fold coordinated by four dipeptide molecules to produce a distorted octahedral geometry (Figure 1a). They can be divided into two types of linkers disposed in a *cis* configuration; two peptides interact through the monodentate C-terminus Thr carboxylate group and the other two forming a five-membered chelate with the amine and oxo groups belonging to the N-terminus Gly residue. An intralayer hydrogen bond between the -OH group from the threonine side chain and the terminal carboxylate group from the same residue (O9–H9···O11, 2.211(2) Å) limits the torsional freedom of this flexible moiety, thus imposing the orientation of the alcohol and methyl groups (Figure 1e). This supramolecular interaction is also responsible for the chelating role played by Gly–Thr and the octahedral coordination of the Zn^{2+} center in **1**, in contrast with the non-chelated tetrahedral coordination of the metal in $[Zn(Gly–Ala)_2]$. As a result, the peptide adopts a conformation defined by values of −141.4(3) and −174.6(2)° for the torsion angles Φ and Ψ, respectively. Comparison of these values with those encountered in $[Zn(Gly\text{-}Ala)_2]$ show that whilst the torsion angle associated with the C-terminus residue (Φ) remains almost constant in both frameworks, that of the N terminus residue (Ψ) is considerably different (see Supporting Information S9). Chelation also imposes a smallest intralayer Zn–Zn distance of 9.078 Å in comparison with the longer 10.130 Å driven by the introduction of Gly–Ala, with the subsequent reduction of the intrinsic porosity in **1** (see below).

Each dipeptide acts as a μ_2-linker connecting two metal ions to form two-dimensional grid-like layers along the *b* axis (Figure 1b). These are packed along the *a* axis following an ..AA.. pattern (Figure 1c) and defining one-dimensional channels which are occupied by methanol guest molecules

[*] Dr. C. Martí-Gastaldo, Dr. J. E. Warren, Dr. K. C. Stylianou, N. L. O. Flack, Prof. M. J. Rosseinsky
Department of Chemistry, University of Liverpool
Crown Street, Liverpool, L69 7ZD (UK)
E-mail: m.j.rosseinsky@liverpool.ac.uk

[**] Financial support from EPSRC under EP/H000925 C.M.-G. thanks the EU for a Marie Curie Fellowship (IEF-253369). We thank C. Aches and R. Athay (Rigaku) for help in developing CCVT.

Supporting information for this article is available on the WWW under http://dx.doi.org/10.1002/anie.201203929.

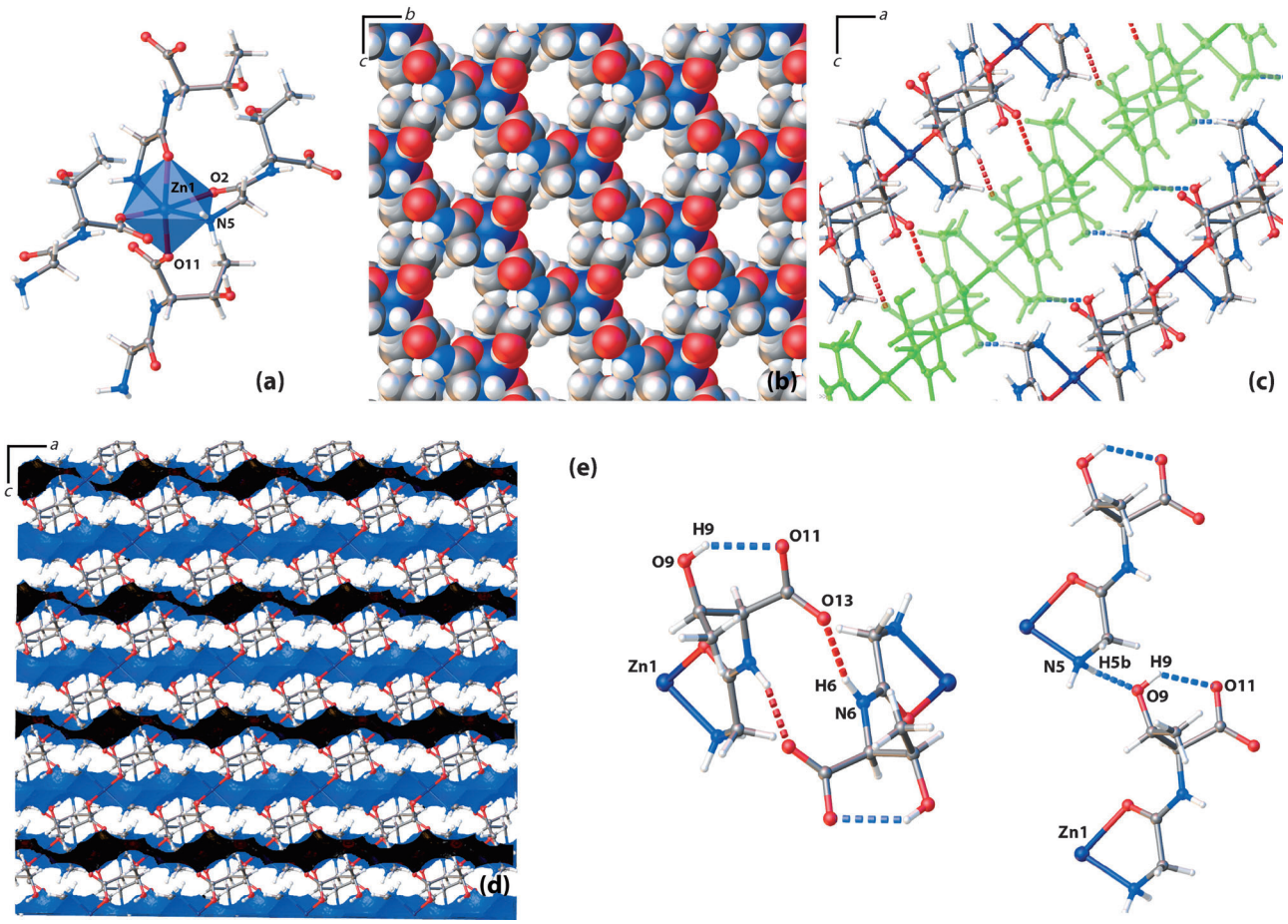

Figure 1. a) Octahedral coordination of the peptide around the zinc(II) ion. b) Space-filling representation showing the grid-like structure of $[Zn(Gly–Thr)_2]$ along the *a* axis. c) Interlayer hydrogen-bonding interactions (represented by dashed lines) between adjacent layers that determine their ..AA.. stacking pattern in the solid-state. Red and blue lines stand for the hydrogen bonds between N–H and C=O groups, that define a H-bond pattern reminiscent of parallel β-sheet packing, and the additional hydrogen bond between the N-terminus amino groups and the -OH side chain from the threonine residue, respectively. For the sake of clarity these have been represented separately and the central layer has been highlighted. d) One-dimensional channels running parallel to the *100* direction across the framework. e) Interlayer hydrogen bonds between N6–H6···O13 and N5–H5···O9 (red and blue dashed lines also indicated in (c)), and intralayer (O9–H9···O11) H-bonds specific to the presence of the threonine side chain (dashed blue lines). Zn dark blue, O red, C gray, N blue, H white.

in the as-prepared material . This arrangement is driven by the presence of parallel H-bonds between the peptide N–H and C=O groups belonging to neighboring layers, defining a pattern reminiscent of the parallel β-sheet interconnecting adjacent beta strands in the secondary structure of proteins. The H-bond network is completed by the interaction between the N-terminus amino groups and the -OH groups from the threonine side chain (Figure 1c and e). This interaction, that is specific to the presence of Thr in the framework, operates between adjacent layers and reinforces the structural stability of the solid in the three dimensions as result of a higher cooperativity. In fact, this additional H-bond is not present in $[Zn(Gly\text{-}Ala)_2]$ and stands as one of the potential causes for the enhanced rigidity of **1** with respect to the previously reported material (see below).

As illustrated in Figure 1d, complete removal of the guest molecules results in 1D channels running parallel to [100]. According to the structural analysis,[11] these account for a solvent-accessible volume of 14.7% of the total volume of **1** (138 $Å^3$ per unit cell at 100 K; see S12 for further details). The resulting porosity exhibits an asymmetric topography. This arrangement is dictated by the O9–H9···O11 intralayer H-bond, that forces the terminal methyl group of the side chain from the α-carbon of the L-threonine component to be projected into the channels. Hence, two methyl groups from the same side of the channel promote the appearance of protuberances in the surface of the pore, thus conferring on it a saw tooth shape; these protuberances are occupied by methanol molecules in the solvated structure (Figure 2).

The composition of **1** as refined from single-crystal X-ray diffraction data is $[Zn(Gly–Thr)_2]\cdot CH_3OH$. This is in good agreement with the solvent content estimated with CHN elemental analysis and thermogravimetric analysis (TGA; S14). Phase purity was confirmed by powder X-ray diffraction (PXRD; S15). It is soluble in water and non-soluble in common organic solvents, such as acetone, EtOH, MeOH, or CH_2Cl_2.

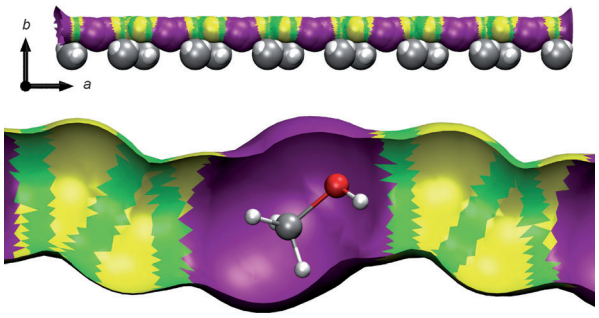

Figure 2. Asymmetric topography of the 1D channels as result of the orientation of the terminal methyl group (gray) from the -CH(OH)CH_3 side chain of the Thr unit (top). The resulting pockets are filled with methanol molecules in the solvated structure (bottom). Colors stand for the probe diameter: green < 2.80 Å > yellow < 2.90 Å > purple.

Compound **1** can be exposed to ambient conditions with no appreciable structural change with time. This structural rigidity contrasts with that displayed by [Zn(Gly-Ala)$_2$], which requires storage under inert conditions to prevent structural transformation as result of the sequential replacement of MeOH guest molecules with atmospheric water vapor. The structure of [Zn(Gly-Thr)$_2$] remains unchanged after activation methods typically used for more rigid "classic" MOFs. Figure 3 shows how the PXRD of the desolvated framework (**1′**), prepared by the evacuation of **1** at 100 °C under dynamic vacuum (10^{-6} mbar) overnight, remains equivalent to that of the as-made material. This robustness drastically differs from the loss in crystallinity and

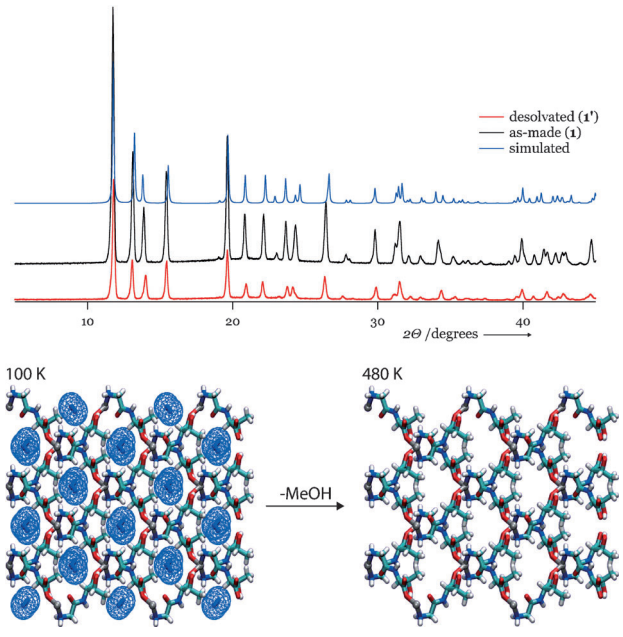

Figure 3. Top: PXRD patterns of the as-synthesized material (**1**), the desolvated framework after overnight evacuation (**1′**) and the profile simulated from the single-crystal data. See S15 and S16 for the unit cell parameters. Bottom: Structure of the framework before and after desolvation as refined from the in situ collection of variable-temperature diffraction data at 100 and 480 K.

significant changes in X-ray scattering observed in the adaptable [Zn(Gly–Ala)$_2$].[12]

Diffraction data was collected between 100 and 500 K. The variable-temperature data collections were undertaken using CCVT, a newly distributed diffractometer and cryostream control program that allows for the automated collection of data from a predetermined library of experiments coupled to the variable of temperature.[13] The crystallinity of the material is retained over the whole temperature range until 500 K, where Bragg diffraction is lost and the structure cannot be determined. The unit cell and crystal structure were determined for each data set by using standard methods and correlated with the guest removal as defined by the occupancy factor of the methanol molecule. This occupancy factor slowly decreases from 100 K to 320 K where it abruptly drops to zero. This temperature is in excellent agreement with that for which complete solvent removal is observed from the TGA data. The associated changes in unit cell dimensions (S18) over this temperature range are very small thus confirming the rigidity of the framework. This behavior substantially differs from the lack of rigidity offered by [Zn(Gly–Ala)$_2$] and, as already pointed out in the structural description, can be associated with the presence of Thr in the dipeptide linker. Hence, it is the presence of hydroxy groups in the side chain of this amino acid that enables the formation of inter and intralayer H-bonds that reinforce the structural stability of **1** in the solid-state and favors the formation of a chelate between the peptide and the metal ion. The potential torsional flexibility of the peptide is thus locked by the combined effect of hydrogen-bonding and chelation, which makes Gly–Thr behave as a rigid connector in sharp contrast with the flexibility provided by Gly–Ala.

We produced crystalline nanosheets of this material by sonomechanical exfoliation of the bulk macroscopic crystals. This strategy has proven to be successful for other layered inorganic material[14] but still remains almost unexplored for MOFs.[15] Stable colorless emulsions of neutral [Zn(Gly–Thr)$_2$] layers were obtained by sonicating a suspension of the dried solid in acetone ([1 g L^{-1}]). This results from the intercalation of the acetone molecules between the layers to disrupt interlayer H-bonds. The presence of exfoliated nanosheets was confirmed by the appearance of Tyndall-like light scattering of the colloid when irradiated with a laser beam (Figure 4a). The size of the exfoliated layers in the acetone dispersion was obtained from dynamic light scattering (DLS) and shows a narrow distribution centered around 140 nm (Figure 4b). Their morphology was studied by atomic force microscopy (AFM). The images were collected by depositing a drop of a freshly prepared diluted emulsion of **1** onto a clean Si wafer. Figure 4c shows a 2 × 2 μm area and demonstrates the presence of rounded particles with lateral sizes consistent with those extracted from the DLS experiments. The lateral thickness of these nanosheets corresponds to an average height profile of 1 nm as illustrated in Figure 4d. This value is close to the crystallographic thickness of a single layer (0.67 nm) and suggests the presence of single-layers accompanied by adsorbed solvate molecules.

Permanent porosity of **1′** was confirmed by CO_2 adsorption at 195 K up to 1 bar. A freshly prepared sample of **1** was

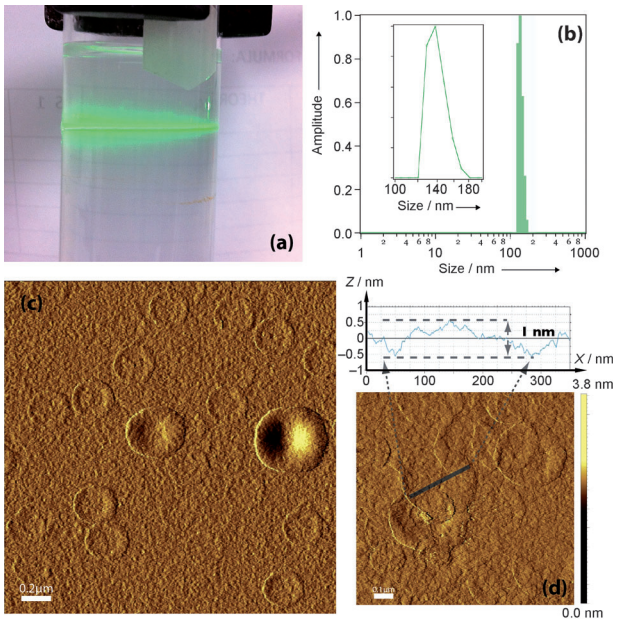

Figure 4. a) Tyndall effect exhibited by the dispersion obtained by sonicating **1** in acetone; b) Number distribution extracted from the DLS study. The inset is an expansion of the highlighted area; c) AFM image of the exfoliated $[Zn(Gly–Thr)_2]$ nanosheets as deposited on a silicon wafer substrate; scale bar = 0.2 μm. d) expansion showing the lateral thickness (along the black line) in good agreement with the expected value for a single layer; scale bar = 0.1 μm.

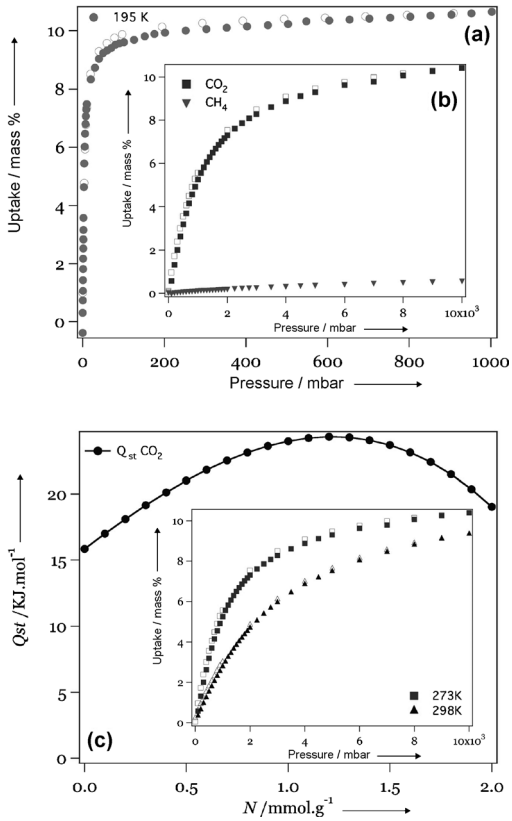

Figure 5. a) CO_2 isotherms of **1** at 195 K (circles). b) Selective sorption of CO_2 (squares) over CH_4 (inverted triangles) at 273 K. c) CO_2 isosteric heat of adsorption calculated from the adsorption branches at 273 (squares; inset) and 298 K (triangles; inset). Filled and empty symbols stand for adsorption and desorption, respectively.

evacuated overnight in an intelligent gravimetric analyzer (IGA) at 80 °C and 10^{-6} mbar. Figure 5a shows a rapid increase of the CO_2 mass uptake at low pressures to reach a plateau with a maximum value of 10.7 wt %. According to the IUPAC standards,[16] this response can be classified as a typical Type I adsorption curve. The data were fitted to the Brunauer–Emmett–Teller (BET) model in the $p/p^0 = 0.02$–0.16 interval to give a BET surface area of 192 $m^2 g^{-1}$. Fitting of the isotherm data to the Dubinin–Radushkevich (DR) equation provides a micropore volume of 0.103 $cm^3 g^{-1}$ (S18)[17] consistent with the value of 0.093 $cm^3 g^{-1}$ estimated from the desolvated crystal structure at 480 K. CO_2 isotherms at 298 and 273 K were collected up to 10 bar (inset Figure 5c). They exhibit a Type I profile with a less-abrupt adsorption at low pressures and, as expected for higher temperatures, smaller uptake values at comparable pressures than the 195 K isotherm.

It is worth comparing this behavior to the sorption response of the related peptide-based $[Zn(Gly–Ala)_2]$. Whilst $[Zn(Gly–Ala)_2]$ exhibited an adaptable response of the framework upon guest sorption with the appearance of a gate-opening pressure as result of the flexibility introduced by the dipeptide, **1** behaves as a "classic" rigid porous open framework, which can be clearly ascribed to the conformational rigidity of the Gly–Thr ligand driven by the intralayer hydrogen bonding. This scenario resembles the close relationship between structural flexibility and biological function present in proteins because the rigid/flexible nature of the peptide determines the structural flexibility of the framework and therefore the sorption response of the porous material.

The coverage-dependent isosteric heat of adsorption (*Qst*) was calculated with a virial-type expression (Figure 5c; S21).[18] The enthalpy of adsorption at zero loading is 15.8 kJ mol^{-1}. This value discards strong interaction of the adsorbate with the framework in the pockets as it falls close to the lower limit of the values reported for other MOFs which range from 14.9 to 90 kJ mol^{-1}, for $[Zn(bdc)(bpy)_{0.5}]$ (MOF508b)[19] and $HCu[(Cu_4Cl)_3(BTTri)_8(en)_5]$,[20] respectively. *Qst f*(*N*) increases with the coverage reaching a maximum of 24.3 kJ mol^{-1} ($N = 1.2$ mmol g^{-1}) from where it starts decreasing. This profile deviates from the common behavior, which typically shows a decrease in the *Qst* values upon adsorption owing to the most favorable sites being occupied first, and suggests that there are no preferential adsorption sites in **1**. This result is consistent with the chemical nature of the pores that is controlled by the presence of alkyl chains, these are not particularly attractive to CO_2, which is likely to favorably interact with the more polar groups, such as the amino or hydroxy moieties through quadrupole–dipole interactions.[21]

Compound **1** is non-porous to N_2 (S19). Comparison of the adsorption isotherms of CO_2 and CH_4 at 273 K (Figure 5b), clearly indicates that CO_2 is preferentially sorbed over CH_4 with a single-component separation ratio of 14:1 (wt %:wt %) at 1 bar. While significant, this value is lower to

the highest reported for a metal–organic framework to date under similar conditions: 24:1 for $[Zn_2(bpdc)_2bpe]$ at 298 K and 1 atm.[22]

Given the pore diameter varies from 2.7 to 5.3 Å,[23] and the kinetic diameters of the gases studied (3.3, 3.64–3.8, and 3.8 Å for CO_2, N_2, and CH_4, respectively), we believe that the selectivity is not size-exclusive in origin. Uptake of these molecules will require relaxation of the pores to allow the guests to reach the largest pocket of correct dimensions to accommodate them. The higher quadrupole moment of CO_2 will lead to more intense quadrupole–dipole interactions with the polar amino/hydroxy groups decorating the framework, thus favoring its diffusion through the channels to finally reach the empty pockets, suggesting that the observed selectivity can be attributed to these interactions.

Whilst the dipeptide Gly–Ala behaves as a flexible peptidic unit in the related $[Zn(Gly–Ala)_2]$,[8] Gly–Thr behaves as a rigid connector in **1** and locks its conformational flexibility by forming a chelate with the Zn^{2+} ion and establishing additional H-bonding interactions in the solid-state as result of its specific sequence of amino acids. This work confirms that both type of units, flexible and rigid, can be used in the design of peptide-based metal–organic frameworks and opens the door for the development of an advanced generation of biomimetic materials that might access the fine compromise between robustness and flexibility encountered in proteins, and relevant to their biological function, by combination of both type of units within a single framework.

Received: May 21, 2012
Published online: October 4, 2012

Keywords: adsorption · metal–organic frameworks · nanoporous materials · peptides · structure–activity relationships

[1] a) See special issue on Metal–Organic Frameworks, *Chem. Rev.* **2012**, *112*, 673–1268; b) S. Kitagawa, R. Kitaura, S.-I. Noro, *Angew. Chem.* **2004**, *116*, 2388–2430; *Angew. Chem. Int. Ed.* **2004**, *43*, 2334–2375.
[2] J. R. Li, R. J. Kuppler, H. C. Zhou, *Chem. Soc. Rev.* **2009**, *38*, 1477–1504.
[3] J.-Y. Lee, O. K. Farha, J. Roberts, K. A. Scheidt, S. B. T. Nguyen, J. T. Hupp, *Chem. Soc. Rev.* **2009**, *38*, 1450–1459.
[4] C. A. Bauer, T. V. Timofeeva, T. B. Settersten, B. D. Patterson, V. H. Liu, B. A. Simmons, M. D. Allendorf, *J. Am. Chem. Soc.* **2007**, *129*, 7136–7144.
[5] a) R. Vaidhyanathan, D. Bradshaw, J.-N. Rebilly, J. P. Barrio, J. A. Gould, N. G. Berry, M. J. Rosseinsky, *Angew. Chem.* **2006**, *118*, 6645–6649; *Angew. Chem. Int. Ed.* **2006**, *45*, 6495–6499; b) J. Perez Barrio, J.-N. Rebilly, B. Carter, D. Bradshaw, J. Bacsa, A. Ganin, H. Park, A. Trewin, R. Vaidhyanathan, A. Cooper, J. E. Warren, M. J. Rosseinsky, *Chem. Eur. J.* **2008**, *14*, 4521–4532.
[6] a) J. An, S. J. Geib, N. L. Rosi, *J. Am. Chem. Soc.* **2009**, *131*, 8376–8377; b) J. An, O. K. Farha, J. T. Hupp, E. Pohl, J. I. Yeh, N. L. Rosi, *Nat. Commun.* **2012**, *3*, 604.
[7] I. Imaz, M. Rubio-Martínez, J. An, I. Solé-Font, N. L. Rosi, D. Maspoch, *Chem. Commun.* **2011**, *47*, 7287–7302.
[8] J. Rabone, Y. F. Yue, S. Chong, K. Stylianou, J. Bacsa, D. Bradshaw, G. Darling, N. Berry, Y. Khimyak, A. Ganin, P. Wiper, J. B. Claridge, M. J. Rosseinsky, *Science* **2010**, *329*, 1053–1057.
[9] A. Dunker, Z. Obradovic, *Nat. Biotechnol.* **2001**, *19*, 805–806.
[10] E. Ueda, Y. Yoshikawa, N. Kishimoto, M. Tadokoro, H. Sakurai, N. Kajiwara, Y. Kojima, *Bull. Chem. Soc. Jpn.* **2004**, *77*, 981–986.
[11] Parameters calculated with CALCVOID, CALCSOLV as implemented in Olex2: O. V. Dolomanov, L. J. Bourhis, R. J. Gildea, J. A. K. Howard, H. Puschmann, *J. Appl. Crystallogr.* **2009**, *42*, 339–341.
[12] R. Afonso, A. Mendes, L. Gales, *J. Mater. Chem.* **2012**, *22*, 1709–1723.
[13] CCVT Rigaku, **2011**.
[14] a) J. N. Coleman, M. Lotya, A. O'Neill, S. D. Bergin, P. J. King, U. Khan, K. Young, A. Gaucher, S. De, R. J. Smith, et al., *Science* **2011**, *331*, 568–571; b) E. Coronado, C. Martí-Gastaldo, E. Navarro-Moratalla, A. Ribera, S. J. Blundell, P. J. Baker, *Nat. Chem.* **2010**, *2*, 1031; c) Y. Hernandez, V. Nicolosi, M. Lotya, F. M. Blighe, Z. Sun, S. De, I. T. McGovern, B. Holland, M. Byrne, Y. K. Gun'Ko, J. J. Boland, P. Niraj, G. Duesberg, S. Krishnamurthy, R. Goodhue, J. Hutchison, V. Scardaci, A. C. Ferrari, J. N. Coleman, *Nat. Nanotechnol.* **2008**, *3*, 563–568.
[15] a) J. C. Tan, P. J. Saines, E. G. Bithell, A. K. Cheetham, *ACS Nano* **2012**, *6*, 615–621; b) P. Z. Li, Y. Maeda, Q. Xu, *Chem. Commun.* **2011**, *47*, 8436–8438.
[16] F. Rouquerol, J. Rouquerol, K. Sing, *Adsorption by Powders and Porous Solids*, Academic Press, London, **1999**.
[17] Y. K. Tovbin, *Russ. Chem. Bull.* **1998**, *47*, 637–643.
[18] L. Czepirski, J. Jagiello, *Chem. Eng. Sci.* **1989**, *44*, 797–801.
[19] L. Bastin, P. S. Barcia, E. J. Hurtado, J. A. C. Silva, A. E. Rodrigues, B. Chen, *J. Phys. Chem. C* **2008**, *112*, 1575–1581.
[20] A. Demessence, D. D'Alessandro, M. Foo, J. Long, *J. Am. Chem. Soc.* **2009**, *131*, 8784–8786.
[21] D. M. D'Alessandro, B. Smit, J. R. Long, *Angew. Chem.* **2010**, *122*, 6194–6219; *Angew. Chem. Int. Ed.* **2010**, *49*, 6058–6082.
[22] J. Zhang, H. Wu, T. J. Emge, J. Li, *Chem. Commun.* **2010**, *46*, 9152–9154.
[23] Diameters were calculated by using the HOLE software package (release 2.2.002). O. S. Smart, J. M. Goodfellow, B. A. Wallace, *Biophys. J.* **1993**, *65*, 2455–2460.

